Reference Command Optimization for the Transition Flight Mode of a Lift Plus Cruise Vehicle

John L. Bullock*, Sheng Cheng†, Andrew Patterson‡, Michael Acheson§, Naira Hovakimyan¶, and Irene Gregory‖

Advanced air mobility mainly utilizes vehicles that are capable of vertical takeoff and landing (VTOL) for the simplicity of operation and large-scale deployment. However, VTOL vehicles need specialized trajectory and command design for the transition phase, where the vehicles transition between rotor-borne flight and wing-borne flight. Since VTOL vehicles are commonly designed as over-actuated systems for redundancy, one challenge that arises is actuator ambiguity, where it is unclear how to uniquely command actuators for the VTOL vehicle to track a given trajectory. We propose a method to design optimal reference commands for the transition mode. By formulating an l_1-norm cost function on the rotor thrusts of the vehicle, we can achieve economical operation of the rotors such that they only operate when necessary and efficiently utilize the aerodynamics to save energy from reduced rotor actuation. We validate our approach in simulations and show its benefit compared to the commonly used differential flatness-based method.

Nomenclature

θ	=	vehicle pitch orientation (rad)
$\boldsymbol{b_1}, \boldsymbol{b_2}$	=	body frame basis vectors
C_{D_1}	=	drag coefficient in the body frame x direction ($\mathrm{N} \cdot \mathrm{s}^2/\mathrm{m}^2$)
C_{D_2}	=	drag coefficient in the body frame y direction ($\mathrm{N} \cdot \mathrm{s}^2/\mathrm{m}^2$)
C_L	=	lift coefficient ($\mathrm{N} \cdot \mathrm{s}^2/\mathrm{m}^2$)
D_1	=	drag in the body frame x direction (N)
D_2	=	drag in the body frame y direction (N)
$\boldsymbol{e_1}, \boldsymbol{e_2}$	=	world frame basis vectors
g	=	gravitational constant ($\mathrm{m/s}^2$)
$\boldsymbol{F}$	=	net force on the vehicle (N)
J	=	vehicle inertia ($\mathrm{kg} \cdot \mathrm{m}^2$)
$C_{L_0}, C_{L_\theta}, C_{L_{\delta_e}}$	=	constants for calculating lift coefficient
C_{D1_0}, C_{D2_0}	=	constants for calculating drag coefficients
C_{D_k}	=	induced drag factor
L	=	lift force (N)
M	=	Net moment on vehicle ($\mathrm{N} \cdot \mathrm{m}$)
m	=	mass of the vehicle (kg)
$\boldsymbol{p}$	=	vehicle center of mass (m)
$R(\theta)$	=	rotation matrix of the vehicle
T_p	=	pusher thrust in the body frame x direction (N)
T_r	=	rotor thrust in the body frame y direction (N)
δ_e	=	aileron deflection (rad)
$\delta_{T_{r1}}, \delta_{T_{r2}}$	=	thrust from each vertical rotor (N)
δ_{T_p}	=	thrust from the pusher (N)

*Doctoral Student, Department of Electrical and Computer Engineering, University of Illinois Urbana-Champaign

†Postdoctoral Researcher, Department of Mechanical Science and Engineering, University of Illinois Urbana-Champaign

‡Research Engineer, Dynamic Systems and Control Branch, NASA Langley Research Center

§Aerospace Technologist, Dynamic Systems and Control Branch, NASA Langley Research Center

¶Professor, Department of Mechanical Science and Engineering, University of Illinois Urbana-Champaign. AIAA Fellow.

‖NASA Senior Technologist for Advanced Control Theory and Application, Dynamic Systems and Control Branch, NASA Langley Research Center. AIAA Fellow.

u	=	velocity in the body frame x direction (m/s)
v	=	velocity in the body frame y direction (m/s)
V_1	=	speed for a steady airflow over the wing for a steady lift (m/s)
V_2	=	cruise speed (m/s)
x	=	world frame x-position of vehicle center of mass (m)
z	=	world frame z-position of vehicle center of mass (m)

I. Introduction

The concept of Advanced Air Mobility (AAM) involves the use of advanced aerial vehicles that can operate with greater efficiency and flexibility than traditional aircraft. These AAM vehicles are typically designed to be highly maneuverable and agile by integrating both rotor-borne and wing-borne flight modes. Such a design leads to vertical take-off and landing (VTOL) aircraft. The VTOL capability is crucial for AAM vehicles because it simplifies operations and enables them to be deployed on a larger scale, making them ideal for applications such as urban air mobility, medical transport, and cargo delivery.

Since the AAM vehicles are capable of rotor-borne and wing-borne flight, the operation of these vehicles can be categorized into hover, transition, and cruise [1]. Hover and cruise are relatively simple to plan for trajectory of flight and control tasks owing to the knowledge and experience documented in the vast literature for multirotor [2–6] and fixed-wing vehicles [7–9], respectively. However, the transition phase poses challenges from two perspectives: trajectory generation and tracking control. The challenges originate in part from the redundant design of the actuators of VTOL vehicles for safety reasons, where the available actuators at the transition phase are the collection of available actuators for rotor-borne and wing-borne flights. A natural question follows: How to design the actuators' reference commands (e.g., thrust and pitch angle) such that the VTOL vehicle can track a given trajectory, especially for the transition between pure rotor-borne flight and wing-borne flight?

Differential flatness has been widely applied in the trajectory generation and computation of reference commands for multirotor vehicles [2, 3, 6], fixed-wing aircraft [10], and VTOL vehicles with specific mechanical structures [11–14]. A system is differentially flat, loosely speaking, if it has enough outputs (or state variables) and control inputs such that all of its state variables and inputs can be expressed as functions of a smaller set of "flat outputs" and their derivatives with respect to time. By parametrizing the flat outputs as polynomial functions in time, one can obtain a compact representation of the desired state and even control inputs. Optimization-based approaches have also proved to be effective in solving the reference commands for trajectory tracking. In [15] and [16], the authors formulate an optimization problem for a winged eVTOL to optimize the pitch and thrust of the vehicle subject to a trajectory tracking constraint on the forces. This work has served as the main motivation for developing the optimization formulation covered in this paper.

In this paper, we propose to utilize optimization to find suitable reference commands for a Lift + Cruise VTOL vehicle to track a given trajectory in the transition phase. A unique feature of the Lift + Cruise vehicle is that it is equipped with uplifting rotors for rotor-borne flight and a horizontally placed pusher for wing-borne flight. Although differential flatness holds for both types of flights individually (i.e., when either using uplifting rotors or pushers), actuation ambiguity will happen when both rotors and pushers are used in the transition mode between pure rotor-borne or wing-borne flights. By ambiguity, we refer to the situation where the reference commands for rotors and pushers cannot be uniquely determined, given the reference trajectory of the vehicle. One could specify the pitch angle of the vehicle to resolve the ambiguity, but designing the pitch angle is not trivial [12]. Instead, we use an optimization method to solve for the reference commands for the thrusts of rotors and pushers as well as the pitch angle simultaneously. We use an l_1-norm equivalent cost function on the thrusts of the rotors and pusher to enforce sparsity [17] on these actuators in the sense that they will operate only when necessary. Such a design will save the energy expenditure during the transition flight for economic power consumption. We further show that the formulation can include the ailerons' reference command as another optimization variable to facilitate the transition flight close to the cruise mode. We validated our approach in simulations to show satisfactory open-loop tracking of the designed trajectory for both hover-to-cruise and cruise-to-hover transitions.

We use a 2D simplified Lift + Cruise model for our study. The paper is organized as follows. The dynamics of the 2D Lift + Cruise vehicle are presented in Section II. Section III discusses the division of the transition mode into two sub-modes: near-hover transition and near-cruise transition. Our optimization problem is shown in Section IV. Section V includes the simulation results, in which we compare our method with the differential flatness method. Lastly, Section VI concludes this paper and summarizes future work.

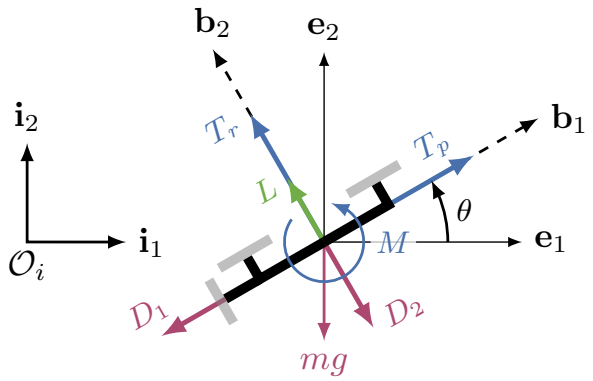

Fig. 1 Free body diagram of a 2D Lift + Cruise vehicle.

II. Dynamics

We will utilize the free body diagram in Fig. 1 to develop the equations of motion for a 2D reduced Lift + Cruise vehicle. The vehicle structure is shown in black, with rotor disks shown as gray rectangles. The forces and moments acting on the vehicle are shown as colored arrows. The blue arrows indicate the forces and moments that are directly controlled. The green arrow represents the aerodynamic lifting force, influenced by wind speed and control surface deflection. Here, we assume that the relative wind that produces the aerodynamic lift always comes in from the direction of the vehicle's heading, i.e., $-b_1$ in Fig. 1. The red arrows denote the drag and gravitation forces that must be overcome by the controller.

The basic 2-dimensional equations of motion are

$$m\ddot{\boldsymbol{p}} = R(\theta)\boldsymbol{F} - mg\boldsymbol{e_2}, \tag{1a}$$

$$J\ddot{\theta} = M. \tag{1b}$$

The net force acting on the vehicle center of mass can be computed as

$$F = (T_p - D_1)\boldsymbol{b_1} + (T_r + L - D_2)\boldsymbol{b_2}. \tag{2}$$

We utilize the following polynomial models to represent the lift and drag forces acting on the Lift + Cruise vehicle:

$$D_1 = u^2 C_{D_1}, \tag{3a}$$

$$D_2 = v^2 C_{D_2}, \tag{3b}$$

$$L = u^2 C_L, \tag{3c}$$

where u and v denote the wind speed on the $-b_1$ and $-b_2$ directions, respectively. We use the following equations for computing the aerodynamic coefficients (which are assumed to be constants):

$$C_L = C_{L_0} + C_{L_\theta}\theta + C_{L_{\delta e}}\delta_e, \tag{4a}$$

$$C_{D_1} = C_{D1_0} + C_{Dk}C_L^2, \tag{4b}$$

$$C_{D_2} = C_{D2_0}, \tag{4c}$$

where δ_e stands for the deflection angle of the aileron. The pusher thrust is generated by the pusher propeller denoted by δ_{T_p}. The forces produced by the two vertical rotors are denoted by $\delta_{T_{r1}}$ and $\delta_{T_{r2}}$. In other words, $T_p = \delta_{T_p}$ and $T_r = \delta_{T_{r1}} + \delta_{T_{r2}}$. The moment M can be generated from the difference in thrust between the two vertical rotors $\delta_{T_{r1}}$ and $\delta_{T_{r2}}$.

III. Sub-modes in the Transition Mode

The transition phase/problem can be defined as the process where the VTOL vehicle transitions between pure rotor-borne flight (hover) and pure wing-borne flight (cruise), e.g., see [1]. Characteristically, the difference between

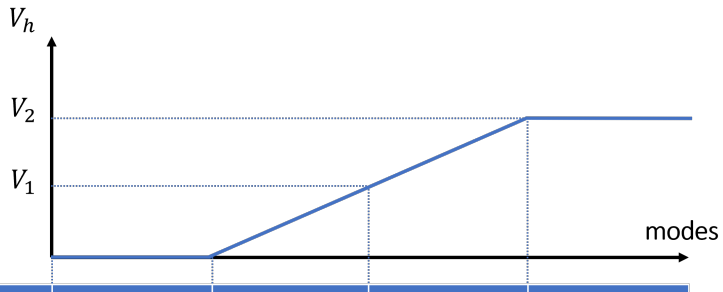

Actuation		Hover	NHT	NCT	Cruise
lift	major	$\delta_{T_{r1}}, \delta_{T_{r2}}$	$\delta_{T_{r1}}, \delta_{T_{r2}}$	δ_{T_p}	δ_{T_p}
	auxiliary	-	-	$\delta_{T_{r1}}, \delta_{T_{r2}}$	-
moment	major	$\delta_{T_{r1}}, \delta_{T_{r2}}$	$\delta_{T_{r1}}, \delta_{T_{r2}}$	δ_e	δ_e
	auxiliary	-	-	$\delta_{T_{r1}}, \delta_{T_{r2}}$	-

Fig. 2 Illustration of the modes of the Lift + Cruise vehicle and associated active actuators for producing necessary forces and moments. V_1 **and** V_2 **stand for speed for a steady airflow over the wing for a steady lift and cruise speed, respectively.**

these two modes can be distinguished by the vehicle's horizontal speed V_h: when the speed is zero or small, the major lift to counteract the gravity comes from the rotors; when the speed accumulates to bigger than the speed V_1, a sustained lift can build up on the wing, albeit not sufficiently large to counteract the gravity; when the speed is large enough to produce lift from the wing to counteract the gravity, then it operates in cruise mode. Hence, the horizontal speed will be used as a critical variable based on which we define the transition mode as $V_h \in [0, V_2]$, where V_2 stands for the cruise speed.

Following this idea, we can further decompose the transition phase into two sub-modes: near-hover-transition (NHT) and near-cruise-transition (NCT) (see the illustration in Fig. 2).

1) NHT: This phase begins with zero horizontal speed and ends when the horizontal speed reaches V_1, at which point the steady airflow can create a steady lift (though not as large as the gravity) on the wing. The major vertical forces are generated from the rotors $\delta_{T_{r1}}, \delta_{T_{r2}}$ (while they also control the pitch angle). The pusher δ_{T1} is kept on to provide horizontal acceleration.
2) NCT: In this phase, the VTOL continues to accelerate horizontally until the horizontal speed reaches the cruise speed V_2, at which time the NCT ends, and the vehicle will transition into the cruise mode. In this phase, major lifts are generated from the wing while the rotors $\delta_{T_{r1}}$ and $\delta_{T_{r2}}$ provide the auxiliary thrust to make up for the remaining lift needed for a designated vertical motion. The pitch angle is controlled by the elevator δ_e, which can also be deflected to facilitate lift on the wing. The pusher δ_{T_p} will continue to provide horizontal acceleration.

Note that the pitch angle should be kept small in these two sub-modes. One reason is that the initial mode (hover) and terminal mode (cruise) of the Lift + Cruise vehicle are both ideally operating subject to a small pitch angle. Restrictions on the pitch angle help to ensure that the vehicle operates smoothly in the transition region, and does not experience large variations in pitch. Another reason is that a large pitch angle will cause waste of actuation when the pusher δ_{T_p} and rotors $\delta_{T_{r1}}, \delta_{T_{r2}}$ are operating at the same time. If the vehicle pitches up too high (Fig. 3a), then a significant portion of T_p is discounted by T_r when these two forces are projected to the horizontal direction. If the vehicle pitches down too low (Fig. 3b), then a significant portion of T_r needs to compensate for the downward projection of T_p to maintain the designated course in the vertical direction. Thus, the Lift + Cruise vehicle should ideally operate in a condition of pitch angle θ close to zero (e.g., Fig 3c) to avoid the waste of actuation for a more energy-efficient flight.

IV. Optimization for Reference Command

In this paper, we want to obtain the reference commands (pusher thrust T_p, rotor thrust T_r, pitch angle θ) such that the 2D Lift + Cruise vehicle can track a given trajectory described in the inertial frame. A commonly used approach for generating the reference commands is to use the differential flatness of a system (if it has the differential flatness

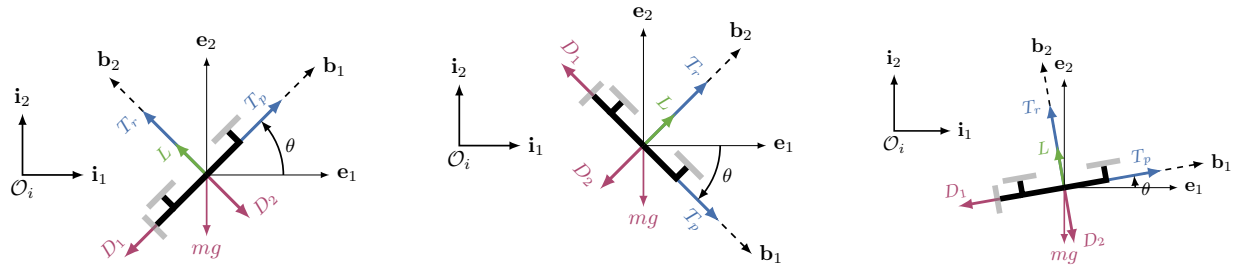

(a) Overly pitching up leading to rotor thrust T_r canceling out pusher thrust T_p's contribution to horizontal acceleration.

(b) Overly pitching down leading to rotor thrust T_r compensating for the downward forces by the pusher thrust T_p.

(c) Small pitch angle helping the rotor and pusher thrusts to coordinate on lifting and horizontal accelerations, respectively.

Fig. 3 Illustration of a suitable pitch angle for energy efficient flight of Lift + Cruise vehicle in the transition mode.

property). Specifically, a system is differentially flat if one can find a set of outputs (equal in number to that of the inputs) such that all states and inputs can be determined from these outputs without resorting to integration. Mathematically, suppose the system has state $x \in \mathbb{R}^n$ and input $u \in \mathbb{R}^m$; then we say the system is flat if we can find outputs $y \in \mathbb{R}^m$ of the form $y = y(x, u, \dot{u}, \ldots, u^{(p)})$ such that $x = x(y, \dot{y}, \ldots, y^{(q)})$ and $u = u(y, \dot{y}, \ldots, y^{(q)})$ [18]. We call y the differentially flat output.

Differential flatness has been shown to exist for multiple types of aircrafts [2, 3, 6, 10–12]. For the 2D Lift + Cruise vehicle, we can choose the (horizontal and vertical) position of the vehicle (x, z) and the pitch angle θ. Assuming the position trajectory on (x, z) is twice continuously differentiable (e.g., represented by Bézier curves). The reference commands can be determined by the following equations:

$$
\begin{aligned}
T_p &= m\big(g\sin(\theta) + \ddot{x}\cos(\theta) + \ddot{z}\sin(\theta)\big) + 2C_{D1_0}\dot{x}^2\cos^2(\theta)\cdot\operatorname{sgn}(\dot{x}\cos(\theta)),\\
T_r &= m\big(g\cos(\theta) - \ddot{x}\sin(\theta) + \ddot{z}\cos(\theta)\big) - \sqrt{\frac{C_{D1_0}}{C_{Dk}}}\dot{x}^2\cos(\theta) + C_{D2}\dot{z}^2\cos^2(\theta)\cdot\operatorname{sgn}(\dot{z}\cos(\theta)),\\
\delta_e &= \frac{\sqrt{\frac{C_{D1_0}}{C_{Dk}}} - C_{L0}}{C_{L_{\delta e}}}.
\end{aligned}
\tag{5}
$$

Here, θ must be known to assign the thrust vector to track the trajectory. This is distinctive to the multirotor's differential flatness property, where one can determine T_r and θ simultaneously from the position trajectory (although one can use the multirotor's differential flatness-based derivation to compute the reference commands for the hover mode of Lift + Cruise vehicle). The extra actuation capability T_p (compared to the multirotor vehicles) introduces the ambiguity in the actuation for which one needs to specify θ. However, it is not straightforward to design θ, whereas designing the position trajectory is almost trivial (the simplest method can be to specify waypoints on the flight path and use Bézier curves to connect them to a smooth trajectory).

In the second method for generating reference commands, we will use optimization to resolve the ambiguity resulting from extra actuation capability. Our approach will find the thrust commands and pitch for the Lift + Cruise vehicle to track the desired path at each individual sample time. The problem minimizes the sum of the pusher thrust T_p and rotor thrust T_r to achieve minimum effort to track the designated trajectory. The path-following is encoded as a constraint in (6), such that the vector sum of the body-frame thrusts and aerodynamic forces will generate the desired force F_{des} in the inertial frame to track the desired trajectory. The other constraints on the optimization problem are imposed to ensure realistic thrust and pitch values throughout the flight.

$$
\begin{aligned}
\min_{T_p, T_r, \theta} \quad & T_p + T_r \\
\text{s.t.} \quad & \theta_{\min} \le \theta \le \theta_{\max}, \\
& T_p \ge 0, \;\; T_r \ge 0, \\
& R(\theta)^T F_{\text{des}}(x_{\text{des}}, z_{\text{des}}) = \begin{pmatrix} T_p \\ T_r \end{pmatrix} + \begin{pmatrix} -D_1(\theta) \\ L(\theta) - D_2 \end{pmatrix},
\end{aligned} \tag{6}
$$

where the desired aerodynamic force can be computed based on the desired position $(x_{\text{des}}, z_{\text{des}})$ and their derivatives, and $R(\theta)$ denote the rotation matrix from the body to inertial frame.

Based on the formulation in (6), we also include the aileron deflection δ_e as an optimization variable, as shown in (7). Adding δ_e as an optimization variable provides more flexibility over the aerodynamic forces on the VTOL. This further enhances the contribution of the aerodynamic forces towards generating the desired forces on the VTOL.

$$
\begin{aligned}
\min_{T_p, T_r, \theta, \delta_e} \quad & T_p + T_r \\
\text{s.t.} \quad & \theta_{\min} \le \theta \le \theta_{\max}, \\
& \delta_{e,\min} \le \delta_e \le \delta_{e,\max}, \\
& T_p \ge 0, \;\; T_r \ge 0, \\
& R(\theta)^T F_{\text{des}}(x_{\text{des}}, z_{\text{des}}) = \begin{pmatrix} T_p \\ T_r \end{pmatrix} + \begin{pmatrix} -D_1(\theta, \delta_e) \\ L(\theta, \delta_e) - D_2 \end{pmatrix}.
\end{aligned} \tag{7}
$$

Note that the cost function used in the above two optimization problems (6) and (7) can be written as $|T_p| + |T_r|$ without changing the outcome of the optimization. This equivalent cost formulation uses l_1-norm in the cost function, which encourages sparsity [17], i.e., the optimization looks for the "simplest" thrust combination on the rotors and pusher to generate the aerodynamic forces specified by the desired trajectory. In other words, the l_1-norm encourages either thrust to become exactly zero, effectively leading to the pusher or rotor to operate only when necessary. With the constraints considered in the optimization problem, the most suitable values of the pitch angle (and aileron deflection) are obtained following the sparsity on the thrusts.

V. Simulation Results

In this section, we validate the proposed optimization formulation for generating reference commands for the Lift + Cruise vehicle. The differential flatness method (5) will serve as the baseline command method to follow a desired trajectory. We test both the baseline and optimization approaches in hover-to-cruise and cruise-to-hover transitions. In each case, the reference commands are computed and used as an open-loop command to the vehicle for the tracking task. We also compute the total sum of the pusher and rotor thrusts over the time span of the flight, following a heuristic metric that lower total thrust values are more energy-efficient for the Lift + Cruise vehicle.

For the simulation, the parameters used are shown in Table 1. For the differential flatness method (5), we fix the pitch angle to $\theta = 0$ following the analysis in Section III, which indicates the preference for a small pitch angle for energy-efficient transition mode.

Table 1 Parameters used in the simulation.

Parameter	Value	Parameter	Value	Parameter	Value
C_{L0}	0.4808	$\theta_{\min}$	$-60°$	m	2.28 kg
C_{L_θ}	3.848	$\theta_{\max}$	$60°$	g	9.8 m/s^2
$C_{L_{\delta e}}$	0.2	$\delta_{e,\min}$	$-30°$	Δt	0.125 s
C_{D1_0}	0.027	$\delta_{e,\max}$	$30°$		
C_{D_k}	0.7	C_{D2}	1.85		

Both the hover-to-cruise and cruise-to-hover trajectories are represented by Bézier curves. The hover-to-cruise trajectory passes through the following waypoints sequentially: (0,0) → (0,50) → (187.5,50) → (375,50) m at time

instances (0, 50, 100, 125) s. The cruise-to-hover trajectory passes through the following waypoints sequentially: (-375,50) → (-187.5,50) → (0,50) → (0,0) m at time instances (0, 25, 75, 125) s.

A. Hover-to-Cruise

Figure 4 shows the trajectory and reference commands computed by differential flatness method (5) (left), optimization with fixed aileron $\delta_e = 0$ (middle), and optimization with flexible aileron (right). All three methods can track the desired trajectory shown in the first row. The interval between 50 s and 100 s is when the vehicle transitions from hover to cruise by gradually building up the horizontal speed. For the baseline method, since a neutral pitch angle $\theta = 0$ is provided, the vehicle simply operates with rotors providing lift and pusher providing horizontal acceleration in a decoupled fashion. One can see the ramp-up of the pusher thrust T_p and the corresponding ramp-down of the rotor thrust T_r as the lift force from the wing increases. For the optimization-based methods, the rate of the ramp-up and ramp-down of the pusher thrust and rotor thrust is larger than that of the baseline approach. Moreover, during the 50-100 s transition window, the vehicle first pitches down to about -3° before turning on the pusher. This maneuver builds up the momentum for initial horizontal acceleration. Then, the vehicle pitches up slightly while the pusher ramps up the thrust for more contributions to the lift and horizontal acceleration. During this pitching-up maneuver, the rotor gradually reduces the thrust until full shut-down. Then, the vehicle pitches down to about -1° and throttles down the pusher thrust for the cruise flight beginning around the 100 s. The above flight maneuver is almost identical in the two optimization problems (with aileron δ_e fixed or set as an optimization variable), with a slight difference in the aileron's reference command δ_e in these two cases. However, notice that the elevator deflection is placed to -81.5° in the baseline approach shown in the left column, which is already below the lowest acceptable deflection of -30°. This is a result of differential flatness's incapability of incorporating physical constraints.

Quantitatively, we show the total thrust produced for the hover-to-cruise trajectory using these three methods in Table 2. The smallest value in each column of Table 2 is in bold. This optimization method improves differential flatness when considering the total summed thrust for tracking the hover-to-cruise trajectory. The optimization method manipulates the pitch of the Lift + Cruise vehicle to take advantage of the aerodynamic forces so that the energy expenditure is most efficient. In summary, the optimization with a flexible δ_e is the most thrust-economic with 13% savings compared to the differential flatness method. At the same time, the optimization method does not sacrifice any trajectory-tracking capability.

Table 2 Break down of accumulated thrusts over the hover-to-cruise trajectory. The unit is [N].

Method	Pusher Thrust T_p	Rotor Thrust T_r	Total Thrust
Differential Flatness (5)	**1236.4**	19708.0	20944.4
Optimization w. fixed δ_e (6)	3097.7	**15102.4**	18200.1
Optimization w. free δ_e (7)	3089.1	15102.8	**18191.9**

B. Cruise-to-Hover

Figure 5 shows the trajectory and reference commands computed by differential flatness method (5) (left), optimization with fixed aileron $\delta_e = 0$ (middle), and optimization with flexible aileron (right). All three methods can track the desired trajectory shown in the first row. The interval between 25 s and 75 s is when the vehicle transitions from cruise to hover by gradually slowing down the horizontal speed. For the baseline method, since a neutral pitch angle $\theta = 0$ is provided, the vehicle simply operates with rotors providing lift and pusher providing horizontal acceleration in a decoupled fashion, similar to what has been displayed in the hover-to-cruise scenario. For the optimization-based methods, the maneuvers are almost reversed in time from those shown in the hover-to-cruise trajectory. Notice that in addition to the aileron deflection reaching -81.5° in the baseline approach shown in the left column, the pushed thrust T_p is reversed to produce a negative thrust shortly after 50 s to slow down the vehicle horizontally to a complete stop. This maneuver violates our constraint that the pusher can only provide positive thrust (only pushing, no "pulling"). This behavior further shows differential flatness's incapability of incorporating physical constraints. For the optimization with a flexible aileron (in the right column), the vehicle did not come to a full stop in the horizontal direction for around 100 s, which resulted in a horizontal drift during that landing maneuver after 100 s. This is partially due to our current validation running in an open-loop fashion. We will look into a closed-loop control with the reference commands in future work for better tracking performance.

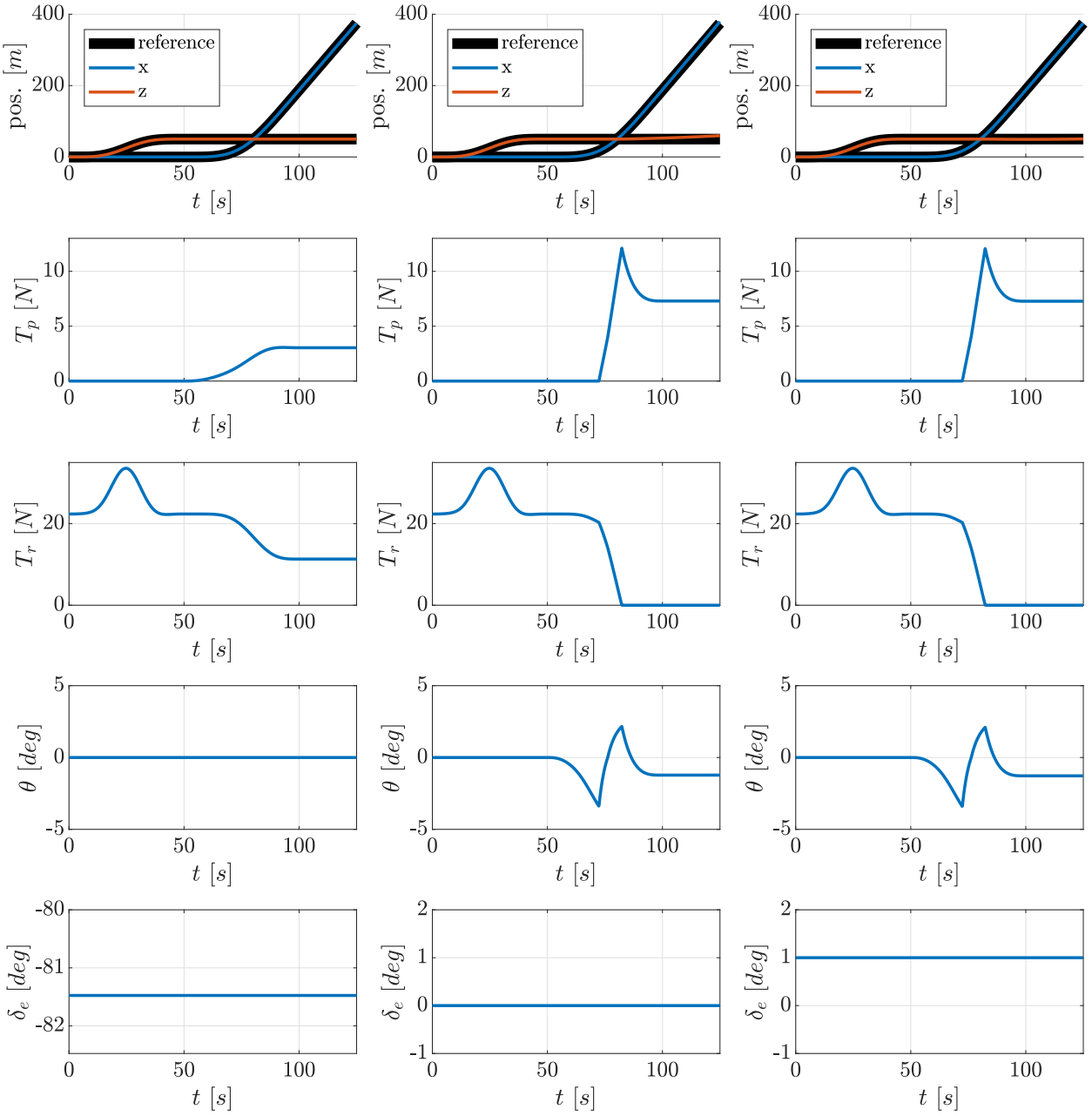

Fig. 4 Trajectory (1st row) and reference commands (2nd-5th rows) for the hover-to-cruise transition computed by the differential flatness method (left column), optimization with fixed aileron ($\delta_e = 0$ in the middle column), and optimization with a flexible aileron (right column).

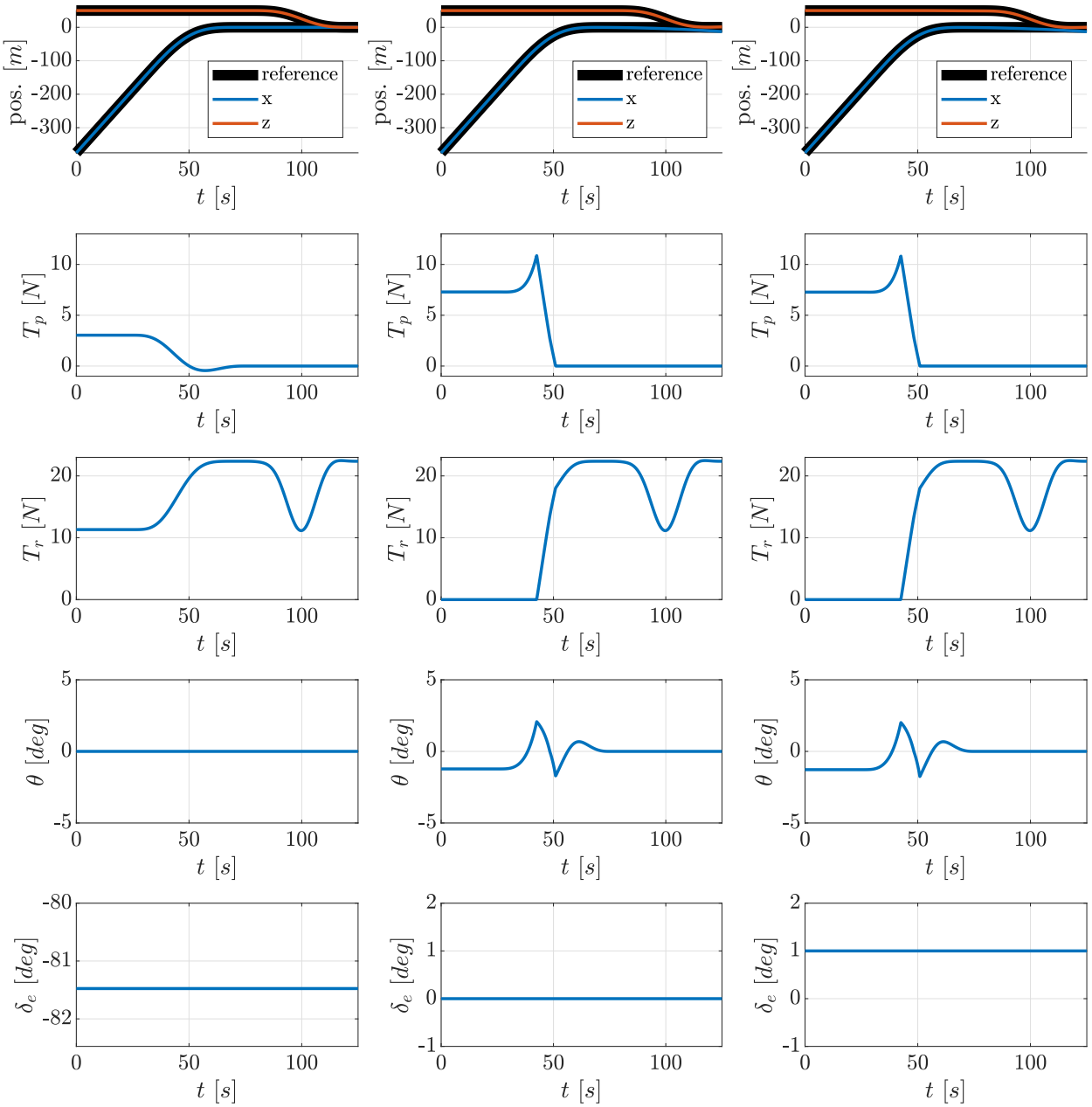

Fig. 5 Trajectory (1st row) and reference commands (2nd-5th rows) for the cruise-to-hover transition computed by the differential flatness method (left column), optimization with fixed aileron ($\delta_e = 0$ in the middle column), and optimization with a flexible aileron (right column).

Quantitatively, we show the total thrust produced for the cruise-to-hover trajectory using these three methods in Table 3. The conclusion is similar to what has been summarized for the hover-to-cruise case in Table 2. In summary, the optimization with a flexible δ_e is the most thrust-economic with 15% savings compared to the differential flatness method.

Table 3 Break down of accumulated thrusts over the cruise-to-hover trajectory. The unit is [N].

Method	Pusher Thrust T_p	Rotor Thrust T_r	Total Thrust
Differential Flatness (5)	**1049.3**	17025.8	18075.1
Optimization w. fixed δ_e (6)	2918.5	**12395.6**	15314.1
Optimization w. free δ_e (7)	2910.2	12395.8	**15306.0**

VI. Conclusion

In this paper, we study the problem of generating reference commands on thrusts and pitch angle for a 2D Lift + Cruise vehicle in the transition mode. We propose an optimization formulation to solve for the reference commands subject to the aerodynamic constraints on the vehicle to track a given flight trajectory that contains the transition between rotor-borne flight and wing-borne flight. Our formulation can resolve the actuation ambiguity issue for the transition flight mode due to extra actuation capability in the Lift + Cruise vehicle while enforcing the sparsity for rotor and pusher thrusts so that they operate only when necessary. We compare our optimization method with the commonly used differential flatness method in simulations. Results indicate that sparsity in the overall thrust leads to more efficient usage of the aerodynamic forces for the transition flight, both in hover-to-cruise and cruise-to-hover transition trajectories. Furthermore, the capability of incorporating constraints in the proposed method shows the advantage in obeying the Lift + Cruise vehicle's physical limits compared to that of the baseline approach.

Future work will investigate an optimization problem at one upper layer [19] that can determine the optimal transition trajectory based on the reference command optimization studied in this paper. We will also look into the controller design associated with tracking the optimal trajectory. Furthermore, we will extend our analysis and design to a 3D Lift + Cruise vehicle.

Acknowledgements

This work is supported by NASA under the ULI grant 80NSSC22M0070.

References

[1] Simmons, B. M., Buning, P. G., and Murphy, P. C., "Full-envelope aero-propulsive model identification for lift+ cruise aircraft using computational experiments," AIAA Aviation 2021 Forum, 2021, p. 3170.

[2] Faessler, M., Falanga, D., and Scaramuzza, D., "Thrust mixing, saturation, and body-rate control for accurate aggressive quadrotor flight," IEEE Robotics and Automation Letters, Vol. 2, No. 2, 2016, pp. 476–482.

[3] Sun, S., Romero, A., Foehn, P., Kaufmann, E., and Scaramuzza, D., "A comparative study of nonlinear mpc and differential-flatness-based control for quadrotor agile flight," IEEE Transactions on Robotics, Vol. 38, No. 6, 2022, pp. 3357–3373.

[4] Goodarzi, F., Lee, D., and Lee, T., "Geometric nonlinear PID control of a quadrotor UAV on SE(3)," 2013 European Control Conference (ECC), IEEE, 2013, pp. 3845–3850.

[5] Lee, T., Leok, M., and McClamroch, N. H., "Control of complex maneuvers for a quadrotor UAV using geometric methods on SE (3)," arXiv preprint arXiv:1003.2005, 2010.

[6] Mellinger, D., and Kumar, V., "Minimum snap trajectory generation and control for quadrotors," 2011 IEEE International Conference on Robotics and Automation, IEEE, 2011, pp. 2520–2525.

[7] Cichella, V., Kaminer, I., Dobrokhodov, V., Xargay, E., Hovakimyan, N., and Pascoal, A., "Geometric 3D path-following control for a fixed-wing UAV on SO(3)," AIAA Guidance, Navigation, and Control Conference, 2011, p. 6415.

[8] Mohamed, A., Massey, K., Watkins, S., and Clothier, R., "The attitude control of fixed-wing MAVS in turbulent environments," Progress in Aerospace Sciences, Vol. 66, 2014, pp. 37–48.

[9] Poksawat, P., Wang, L., and Mohamed, A., "Gain scheduled attitude control of fixed-wing UAV with automatic controller tuning," IEEE Transactions on Control Systems Technology, Vol. 26, No. 4, 2017, pp. 1192–1203.

[10] Bry, A., Richter, C., Bachrach, A., and Roy, N., "Aggressive flight of fixed-wing and quadrotor aircraft in dense indoor environments," The International Journal of Robotics Research, Vol. 34, No. 7, 2015, pp. 969–1002.

[11] Airimitoaie, T.-B., Aguilar, G. P., Lavigne, L., Farges, C., and Cazaurang, F., "Convertible aircraft dynamic modelling and flatness analysis," IFAC-PapersOnLine, Vol. 51, No. 2, 2018, pp. 25–30.

[12] Tal, E., Ryou, G., and Karaman, S., "Aerobatic trajectory generation for a VTOL fixed-wing aircraft using differential flatness," arXiv preprint arXiv:2207.03524, 2022.

[13] Yüksel, B., Buondonno, G., and Franchi, A., "Differential flatness and control of protocentric aerial manipulators with any number of arms and mixed rigid-/elastic-joints," 2016 IEEE/RSJ International Conference on Intelligent Robots and Systems (IROS), IEEE, 2016, pp. 561–566.

[14] McIntosh, K., Reddinger, J., Zhao, D., and Mishra, S., "Optimal trajectory generation for transitioning quadrotor biplane tailsitter using differential flatness," Vertical Flight Society 77th Annual Forum Proceedings, 2021.

[15] Willis, J. B., and Beard, R. W., "Nonlinear trajectory tracking control for winged eVTOL UAVs," 2021 American Control Conference (ACC), 2021, pp. 1687–1692. https://doi.org/10.23919/ACC50511.2021.9482620.

[16] Willis, J. B., and Beard, R. W., "Pitch and thrust allocation for full-flight-regime control of winged eVTOL UAVs," IEEE Control Systems Letters, Vol. 6, 2022, pp. 1058–1063. https://doi.org/10.1109/LCSYS.2021.3089130.

[17] Boyd, S. P., and Vandenberghe, L., Convex Optimization, Cambridge university press, 2004.

[18] Murray, R. M., Rathinam, M., and Sluis, W., "Differential flatness of mechanical control systems: A catalog of prototype systems," ASME International Mechanical Engineering Congress and Exposition, Citeseer, 1995.

[19] Chen, Q., Cheng, S., and Hovakimyan, N., "Simultaneous spatial and temporal assignment for fast UAV trajectory optimization using bilevel optimization," IEEE Robotics and Automation Letters, 2023.